Article:
Pankhurst, MJ, Gueninchault, N, Andrew, M et al. (1 more author) (2019) Non-destructive three-dimensional crystallographic orientation analysis of olivine using laboratory diffraction contrast tomography. Mineralogical Magazine, 83 (5). pp. 705-711. ISSN 0026-461X

https://doi.org/10.1180/mgm.2019.51

Title:

Non-destructive three-dimensional crystallographic orientation analysis of olivine using Laboratory Diffraction Contrast Tomography

Running title:

Pankhurst et al. Crystallographic orientation of olivine in three-dimensions

Authors:

Matthew J Pankhurst[1,2]*, Nicolas Gueninchault[3,4], Matthew Andrews[4], Edward Hill[5]

Addresses:

[1]Instituto Tecnológico y de Energías Renovables (ITER), 38600 Granadilla de Abona, Tenerife, Canary Islands, Spain

[2]Instituto Volcanológico de Canarias (INVOLCAN), INtech La Laguna, Calle Alvaro Diaz n2, 38320 La Laguna, Tenerife, Canary Islands, Spain

[3]Xnovo Technology ApsS, Theilgaards Alle 9, 1.th, Køge, Denmark

[4]Carl Zeiss X-ray Microscopy, 4385 Hopyard Road, Pleasanton, CA, USA, 64588

[5]Carl Zeiss Microscopy Limited, 509 Coldhams Lane, Cambridge, CB1 3JS, UK

Initial submission date:

16/01/2019

Abstract

X-ray Laboratory Diffraction contrast tomography (LabDCT) produces three-dimensional (3D) maps of crystallographic orientation. The non-destructive nature of the technique affords the key benefit of full 3D context of these, and other, in-situ measurements. This study is the first to apply the technique to any material other than a metal or silicon. We report the first 3D measurements of the crystallographic orientation of olivine, which also makes this study the first to apply LabDCT to a) a non-metallic, non-cubic system and b) geological material. First, we scanned fragments of olivine set in resin alongside glass microbeads using LabDCT and Absorption Contrast Tomography (ACT). Then we reconstructed these data assuming an orthorhombic crystal system. We show that a) the regions within the sample that index well according to the orthorhombic system correspond to olivine fragments in the ACT image, b) crystalline regions not corresponding to olivine are not indexed assuming the same lattice parameters, and c) the diffraction data discriminates crystalline from non-crystalline materials as expected. Finally, we demonstrate that the method resolves sub-degree orientation differences between distinct regions within individual olivine fragments. We conclude that DCT can be applied to the study of rocks and other crystalline materials, and offers advantages over conventional techniques. We also note that LabDCT may offer a solution to the crystallographic measurement of substances that would otherwise be difficult to measure due to challenges in obtaining a perfect sample polish. Future developments to accommodate larger experimental volumes and additional crystallographic systems within a sample promises to expand the applicability and impact of DCT.

Keywords:

X-ray diffraction tomography, olivine, 3D imaging, non-destructive.

Footnotes:

*mpankhurst@iter.es

Introduction

Electron Back Scatter Diffraction (EBSD) is the principal method used to measure the orientation *and* spatial distribution of the minerals from which a rock is constructed (see Prior *et al.*, 2009 for a review). This technique has provided great insight into the kinematics of rock deformation (e.g. Trimby *et al.*, 1998; Bestmann and Prior, 2003) metamorphic spotsses (e.g. Spiess *et al.*, 2001, 2007, 2012; Storey and Prior, 2005; Díaz Aspiroz *et al.*, 2007) planetary geology (He *et al.*, 2006) and geochronology (e.g. Reddy *et al.*, 2007; Piazolo *et al.*, 2012; Timms *et al.*, 2012, 2017). EBSD can only be conducted on the surface of a polished sample, and under the vacuum conditions of an electron microscope. It is possible to extend this technique into 3D by coupling with Focussed Ion Beam (FIB) serial sectioning (e.g. Calcagnotto *et al.*, 2010), yet the production of these data is extremely slow and not practical for most applications. Furthermore, as it is destructive, this 3D technique does not allow for samples to be subjected to experimental stress, temperature or deformation which would allow for the direct investigation of geological processes *in situ* within the microscope.

Mapping crystallographic orientations of a polycrystalline sample non-destructively has mainly grown from within material science (Poulsen *et al.*, 2001; Poulsen, 2012) and is now a routine tool implemented in several synchrotrons, like at the ESRF (referred to as “Diffraction Contrast Tomography” Ludwig *et al.*, 2009), APS and CHESS (referred to as “High Energy X-ray Diffraction Microscopy” Lienert *et al.*, 2011). This type of technology has only recently been available using laboratory X-ray sources (the reader interested in the physics are directed to McDonald *et al.*, 2015 and; Holzner *et al.*, 2016), see also Fig. 1. In the first instance, application of LabDCT was limited to the analysis of the grain centre of mass location and orientation of cubic materials (metals; see McDonald *et al.*, 2015).

To make LabDCT possible using such low brilliance polychromatic sources, and to optimize the signal:noise of the images recorded by the detector, diffraction patterns are collected in a specific configuration called “Laue symmetry” where the source to sample and the sample to detector

distances are identical (see Oddershede *et al.*, 2019 for an introduction). A tungsten aperture is inserted between the source and the sample to ensure that the volume of interest is solely illuminated, as well as a square tungsten beamstop in front of the detector to prevent direct beam exposure of the scintillator (Fig. 1).

LabDCT is a fast-developing technique: now the full shape of the grains can be reconstructed from high-fidelity diffraction signals (Bachmann *et al.*, 2019) rather than tessellation (McDonald *et al.*, 2017), which provides improvements to 5D analysis of the grain boundaries network (see Shahani *et al.*, 2017; Oddershede *et al.*, 2019; Sun *et al.*, 2019). The full-grain approach in theory extends the application to any kind of crystalline material (c.f. tessellation which is otherwise restricted due to the lower crystallographic symmetry of a non-cubic material), and with the benefit of multi-modal 3D imaging (see Keinan *et al.*, 2018 and references therein) and improvements to grain mapping reliability (Niverty *et al.*, 2019), supports attempts to conduct LabDCT analysis of more complicated materials, like rocks.

Olivine, which is orthorhombic, dominates the upper mantle by volume, is a prevalent mineral involved in the petrogenesis of basaltic liquids (e.g. Holtzman *et al.*, 2003), crystallises and fractionates in olivine saturated magmas (Pankhurst *et al.*, 2018a), and is common in some meteorite classes (Rudraswami *et al.*, 2016). Olivine is also used as a reactant in some industrial processes (Kemppainen *et al.*, 2012), and is a common slag mineral (Piatak *et al.*, 2015). The crystallographic orientation of olivine in natural rocks provides insights to mantle flow and physical anisotropies (Mizukami *et al.*, 2004; Tasaka *et al.*, 2008; Demouchy *et al.*, 2012; Hansen *et al.*, 2012; Michibayashi *et al.*, 2016), is essential for accurate derivation of 3D olivine element diffusion chronometry (Dohmen *et al.*, 2007; Shea *et al.*, 2015b; a), and provides information as to closed-system kinetics in condensing planetary discs and the formation of rocky bodies (Miyamoto *et al.*, 2009).

Measuring the size, shape, composition and crystallographic orientation of olivine to address research questions normally requires destructive sample preparation (thin section or grain mount) and 2D analysis. The inherent advantages of LabDCT include volume analysis, which bypasses the need to extrapolate 2D crystallographic data into 3D for use in structural interpretation. This also allows for per-voxel linking to 3D chemical information using calibrated X-ray tomographic attenuation images (Pankhurst *et al.*, 2018b); and potentially, to build such datasets faster than would otherwise be feasible with 2D analysis that requires intensive sample preparation and raster-type scanning (Pankhurst *et al.*, 2014). Our primary aim here is to determine whether LabDCT can measure the crystallographic orientation of olivine and gauge the likely uncertainty upon such measurements.

Methods

Experiment design

Numerous fragments of olivine of the same composition were scanned using LabDCT together with glass microbeads set into a resin straw. Setting a limited number of particles into resin held the experiment still and provided the highest possibility of clean diffraction projection images in this first experiment. It also aided us to make clear comparisons between particles as either olivine grains, and that of glass (which by definition should not produce diffraction spots), since we can use the shape of the particle to independently assign the material type.

Sample preparation

Approximately 1 mm wide, 5 mm deep holes were drilled into the walls of a silicon mount under a binocular microscope. The sides of the holes are rough. A single crystal of olivine from San Carlos (characterised previously by Pankhurst *et al.*, 2017) was manually crushed using a pestle and mortar,

and shards ~50 to 300 µm in length were dropped into these holes using tweezers. Glass microbeads (SLGMS-2.5: 45-53 µm, supplied by *Cospheric*; www.cospheric.com) were also introduced.

Two-part epoxy resin Epothin 2 (*Beuhler*; www.buehler.com) was dripped onto the opening of the holes, but did not penetrate due to surface tension. The mount was placed into a vacuum, and then pressure vessel, which was observed to help draw the resin down into the holes. After curing, the silicon mount was manipulated such that the resin poked out from the opening of the holes, which allowed recovery by tweezers. Visual inspection shows that the particles are distributed around the edges of a resin straw, apparently the particles caught by, and resin wicked onto, the rough walls of the bespoke mold.

Sample measurements

At Carl Zeiss X-ray Microscopy, 4385 Hopyard Road, Pleasanton, CA, USA a LabDCT dataset consisting of two tomographic scans was acquired sequentially on a Zeiss Xradia Versa 520 equipped with the LabDCT module (Laue focussing geometry) without disturbing the sample. First, a classic absorption computed tomography (ACT) scan consisting of 2401 projections was collected without any beamstop or aperture, around 360° using a rotation stage. For each image, the exposure time was set to 1 second without any binning. The working distances were both 13 mm, leading to a pixel size of 1.69 µm. The source was set at 160 kV and 10W, and the resulting tomographic volume was reconstructed using a filtered back projection algorithm. For the LabDCT scan, 181 diffraction contrast patterns (DCP) around 360° were collected (every 2° of rotation), with a single exposure time of 600 seconds for a total scan time of 30.17 hours. A 750x750 µm aperture and a 2.5x2.5 mm beamstop were used, set in place automatically and without opening the X-ray instrument (see figure 1).

Data reconstruction and reduction

We reconstructed the absorption data first to confirm that olivine and microbead particles are easily distinguishable by shape. Diffraction data were then reconstructed at a spatial resolution of 2.5 µm and indexed using orthorhombic crystal symmetry, along with a calculation of per-voxel confidence value using the GrainMapper3D® software developed by Xnovo Technology ApS. A brief description of the For a full description of the GrainMapper3D method used here, we direct the reader to Bachmann et al. (2019).

King et al. (2013) showed how using a projection geometry (with sample close to the source but far from the detector), it is possible to non-destructively reconstruct a grain map with a laboratory-based system. In that work, the algorithm relies on the identification of the precession path of the diffraction spots, identifying a maximum of energy to determine the geometry of the diffraction event and, thereafter, determine the orientation of the grain fulfilling the Bragg's condition. This information is later used to reconstruct the grain map using oblique back projection from a SIRT algorithm.

The GrainMapper3D® (Bachmann et al., 2019) used for the current experiment relies on a different method. Here, the sample is placed in "Laue-focusing" geometry, where the source-to-sample and sample-to-detector distances are equal. Consequently, the diffraction spots appear as lines on the detector, which reduce the probability of spot overlaps and require less acquisition time. Once the diffraction dataset is acquired, the spots are then binarized and the algorithm will consider a simplified diffraction model which attempts to optimize a metric called "completeness" locally. The algorithm generates a list of possible grain candidates from the diffraction data, with the *a priori* knowledge of the diffraction geometry, and probe defined locations within the sample's volume while checking for the best grain candidate through a heuristic approach.

The quality of indexing has a natural upper limit due to the potential for diffracted X-rays to be absorbed, or spots to overlap etc.. In practice, the completeness value must be >40% for the solution to be considered, and trusted at 85% using GrainMapper3D®, which corresponds to an uncertainty

within the 95% confidence interval, (see corroboration with EBSD data in Niverty *et al.*, 2019). We used a completeness value of 85% in this study. The data were then reduced by labelling neighbouring voxels of <0.1° misorientation together as distinct regions (i.e. misorientation of >0.1° between two neighbouring voxels places each into different labelled regions), and the results from each region displayed as the average value according to two visualisation schemes: IPF (inverse pole figure) and HKL (Miller indices).

Results and discussion

The conventional absorption data are summarised in figure 2 which illustrates the random distribution of particles set into place by the resin. A single projection of the raw diffraction data is shown in Figure 3a, overlain with the results of a forward model (discussed below). The corresponding reconstructed LabDCT image is presented in Fig. 3b; diffraction spots in Fig. 3a correspond to the same coloured fragment in Fig. 3b.

LabDCT resolves the olivine fragments (shards, generally with concoidal fracture) using an orthorhombic symmetry. These indexed areas match the location, size and shape of olivine fragments in the attenuation image. Glass microbeads, resin nor indeed air, do not produce diffraction spots (Fig. 4).

A surprise result was the (poor) indexing in the orthorhombic system of an anomalously bright region of the attenuation image (Fig. 4). This particle is crystalline, yet is too dense to be the San Carlos olivine. It is not attached to any other particle and does not index as spinel, which is a common dense mineral inclusion in olivine. Since its origin is likely to be contamination further speculation as to its nature is unwarranted, yet it does offer a useful true negative result when compared to the olivine true positive results. It signals that crystalline phases may be distinguishable by LabDCT on the basis of the strength of their indexing according to any one system.

We observe clusters of spots on the raw diffraction data which correspond to distinct volumes within the sample that are proximal to each other, and display distinct crystallographic orientation. This result brings the potential of this technique sharply into focus, since these observations originate from sub-grains within individual fragments, and so demonstrate that subtle variation is detectable (Fig. 5, Table 1). To illustrate the nature of the sub-grain boundaries we visualised the olivine data as pole figures (Fig. 6). In this experiment comprised of randomly located, randomly orientated particles, the distinct clusters of orientation data in Fig. 6 can be traced to single grains of olivine and the spread within a cluster indicates the divergence of sub-grains. We consider that interpretation beyond these observations is better directed at samples that have not been crushed. Imaging and analysis of such unmodified samples is the subject of current work.

Future potential and challenges

The present study describes the first instance of non-destructive crystallographic orientation analysis of a material with a non-metallic, non-cubic system using LabDCT. An exhaustive comparison against other crystallographic orientation measurement techniques is beyond the scope of this contribution, and will require data from natural samples to be gathered from a range of such techniques to best articulate the advantages and limitations to geoscience. Below is an outline of how this technique could grow, and where barriers to that growth could originate. First we return to a brief comparison between EBSD and LabDCT.

LabDCT is anticipated to become a highly complementary technique to that of EBSD. Here we demonstrate olivine is able to be analysed in 3D and non-destructively, yet there is much development work to be conducted before different crystal systems can be analysed by LabDCT with confidence, which would then allow for a variety of rocks to be examined, like they are routinely using EBSD. Furthermore, the highest spatial resolution possible using EBSD is currently greater than that demonstrated by LabDCT studies, and the width and length of a single map possible by EBSD is over an order of magnitude larger than state of the art LabDCT. Importantly, LabDCT as compared to

EBSD analysis of the same sample finds good agreement in both location and shape of crystallographic domains and orientation accuracy (Niverty *et al.*, 2019). LabDCT has higher angular resolution than EBSD due to the gathering of diffraction data as tracks over large angles whose solution, found during reconstruction, converges at a higher resolution than that of an individual projection. Consistency between grains studied by McDonald et al. (2017) suggest a measurement accuracy of <0.05°, which is shown experimentally by Bachmann (2019). Compare this data gathering geometry to diffraction patterns that are 2D images, where angular resolution is linked to the width of the Kikichi bands and by extension, the depth of focus. EBSD angular resolution is on the order of tenths of degrees (McDonald *et al.*, 2017).

Optimisation

This study's experiment was conducted using typical scan settings used to measure the orientation of grains within metals (Niverty *et al.*, 2019). The only difference to note was that the exposure was set to 600 s per projection rather than the 500 s used by Niverty et al. (2019) in an attempt to maximise the intensity of the olivine diffraction spots. The quality of these first results in terms of the ability to domain voxels with the same orientation are comparable to state-of-the-art EBSD datasets with acceptable mean angular deviation values (Maitland and Sitzman, 2007), see Niverty et al. (2019) who conducted a 1:1 comparison between LabDCT and EBSD data.

For the LabDCT method to gather enough information for complete indexing, weak as well as strong reflections are required to be resolved. As geological crystals are frequently low symmetry, strained and/or twinned at various scales, the typical diffraction spots in future work are anticipated to be weaker, noisier, and more artefact-prone than those generated from metallic samples. The diffraction of the material therefore serves as a limitation to indexation with high confidence. One simple way to optimise what is essentially a segmentation challenge is to increase in exposure time

to improve the signal-to-noise for weakly scattering crystals, yet other options are becoming available.

Recent benchmarking results from the application of modern data science and machine learning techniques shows significant benefits to the identification of individual diffraction spots from a noisy and artefact prone diffraction pattern (e.g. Andrew, 2018; Berg *et al.*, 2018). Such techniques may prove especially valuable when trying to extend diffraction contrast to more complex mineralogical or crystallographic systems (e.g. Darling *et al.*, 2016).

Materials

The crystallography of minerals in solid solutions, like olivine and others including the feldspar group, is effected by their composition (e.g. Deer *et al.*, 1992). Further work is required to determine how chemical variation across a solid solution might effect LabDCT results, to what degree this may be a source of uncertainty (for instance, if the sample is known to contain olivine, but the composition is not known the input lattice parameters must only be an approximation). It is worth nothing that by resolving subgrains within a single particle, the technique can resolve boundaries where distinct grains are touching, as they are frequently observed to be in natural samples. It is also worth noting that crystallographic orientation imparts measurable variations in signal intensity during electron beam analysis whereby a *volume* of excitation produces yield (e.g. as secondary or backscattered electrons or X-rays). Using LabDCT to map the surface and *subsurface* of grain mounts or thin sections may have value in increasing the accuracy of compositional measurement, in particular with respect to spatial characterisation of reference materials (e.g. Pankhurst *et al.*, 2017).

Strained crystals, such as many in nature (see Hunter *et al.*, 2018 for a recent example) as well as those synthesized in laboratory experiments (e.g. Hansen *et al.*, 2012), represent a limitation of, yet also an opportunity for, LabDCT as applied to geoscience. For instance, departure from an idealised crystallographic structure reduces the capacity for software to index the data. This necessarily effects accuracy and precision of the measurement, yet also may indicate the presence of elastic or

plastic strain. The assumption of one orientation per grain is difficult to apply, since generally the diffraction spots lose their shape and start to streak. Mapping this reduction in indexation, or change in spot shape/size for a given material of the same phase and known or controlled shape (in 3D) may constitute a new way forward in understanding the development of strain. It is plausible that this technique may be developed for in-situ use during live/interrupted deformation and/or heating experiments depending on experiment requirements (see McDonald *et al.*, 2017 for an example). These would need to be designed with the scanning duration in mind, yet is still advantageous compared with the impossibility of using 2D, destructive techniques.

Conclusions and implications

This study demonstrates that the crystallographic orientation of olivine can be measured using DCT, which opens new avenues of research upon olivine and, by extension, other non-metallic crystalline materials. The inherent ability of LabDCT to distinguish crystalline from non-crystalline substances in 3D, and potential to use the quality of indexing to different crystallographic systems as a parameter for segmenting 3D image volumes, holds potential to be used to discriminate between phases in natural rocks and other materials. For those minerals that have orthorhombic structures, we show that each grains' crystallographic orientation, and those of any sub-grains, can be determined precisely. We conclude that in addition to metals, LabDCT is applicable to a range of materials. Due to the inherently 3D and non-destructive nature of the technique, promising new directions for research and understanding of the formation and evolution of crystalline materials are now possible.

References

Andrew M. (2018) A quantified study of segmentation techniques on synthetic geological XRM and FIB-SEM images. *Computational Geosciences*, **22**, 1503–1512.

Bachmann F., Bale H., Gueninchault N., Holzner C. and Lauridsen E.M. (2019) 3D Grain reconstruction from laboratory diffraction contrast tomography. *Journal of Applied Crystallography*, **52**, 643–651.

Berg S., Saxena N., Shaik M. and Pradhan C. (2018) Generation of ground truth images to validate micro-CT image-processing pipelines. *The Leading Edge*, **37**, 412–420.

Bestmann M. and Prior D.J. (2003) Intragranular dynamic recrystallization in naturally deformed calcite marble: diffusion accommodated grain boundary sliding as a result of subgrain rotation recrystallization. *Journal of Structural Geology*, **25**, 1597–1613.

Calcagnotto M., Ponge D., Demir E. and Raabe D. (2010) Orientation gradients and geometrically necessary dislocations in ultrafine grained dual-phase steels studied by 2D and 3D EBSD. *Materials Science and Engineering: A*, **527**, 2738–2746.

Darling J.R., Moser D.E., Barker I.R., Tait K.T., Chamberlain K.R., Schmitt A.K. and Hyde B.C. (2016) Variable microstructural response of baddeleyite to shock metamorphism in young basaltic shergottite NWA 5298 and improved U–Pb dating of Solar System events. *Earth and Planetary Science Letters*, **444**, 1–12.

Deer W.A., Howie R.A. and Zussman J. (1992) *An introduction to the rock-forming minerals*. P. in.: Longman London.

Demouchy S., Tommasi A., Barou F., Mainprice D. and Cordier P. (2012) Deformation of olivine in torsion under hydrous conditions. *Physics of the Earth and Planetary Interiors*, **202–203**, 56–70.

Díaz Aspiroz M., Lloyd G.E. and Fernández C. (2007) Development of lattice preferred orientation in clinoamphiboles deformed under low-pressure metamorphic conditions. A SEM/EBSD study of metabasites from the Aracena metamorphic belt (SW Spain). *Journal of Structural Geology*, **29**, 629–645.

Dohmen R., Becker H.-W. and Chakraborty S. (2007) Fe–Mg diffusion in olivine I: experimental determination between 700 and 1,200°C as a function of composition, crystal orientation and oxygen fugacity. *Physics and Chemistry of Minerals*, **34**, 389–407.

Hansen L.N., Zimmerman M.E., Dillman A.M. and Kohlstedt D.L. (2012) Strain localization in olivine aggregates at high temperature: A laboratory comparison of constant-strain-rate and constant-stress boundary conditions. *Earth and Planetary Science Letters*, **333–334**, 134–145.

Holtzman B.K., Kohlstedt D.L., Zimmerman M.E., Heidelbach F., Hiraga T. and Hustoft J. (2003) Melt segregation and strain partitioning: implications for seismic anisotropy and mantle flow. *Science*, **301**, 1227–1230.

Holzner C., Lavery L., Bale H., Merkle A., McDonald S., Withers P., Zhang Y., Jensen D.J., Kimura M., Lyckegaard A., Reischig P. and Lauridsen E.M. (2016) Diffraction Contrast Tomography in the Laboratory – Applications and Future Directions. *Microscopy Today*, **24**, 34–43.

Hunter N.J.R., Weinberg R.F., Wilson C.J.L., Luzin V. and Misra S. (2018) Microscopic anatomy of a "hot-on-cold" shear zone: Insights from quartzites of the Main Central Thrust in the Alaknanda region (Garhwal Himalaya). *GSA Bulletin*, **130**, 1519–1539.

Keinan R., Bale H., Gueninchault N., Lauridsen E.M. and Shahani A.J. (2018) Integrated imaging in three dimensions: Providing a new lens on grain boundaries, particles, and their correlations in polycrystalline silicon. *Acta Materialia*, **148**, 225–234.

Kemppainen A., Mattila O., Heikkinen E.-P., Paananen T. and Fabritius T. (2012) Effect of H2–H2O on the Reduction of Olivine Pellets in CO–CO2 Gas. *ISIJ International*, **52**, 1973–1978.

King A., Reischig P., Adrien J. and Ludwig W. (2013) First laboratory X-ray diffraction contrast tomography for grain mapping of polycrystals. *Journal of Applied Crystallography*, **46**, 1734–1740.

Lienert U., Li S.F., Hefferan C.M., Lind J., Suter R.M., Bernier J.V., Barton N.R., Brandes M.C., Mills M.J., Miller M.P., Jakobsen B. and Pantleon W. (2011) High-energy diffraction microscopy at the advanced photon source. *JOM*, **63**, 70–77.

Ludwig W., Reischig P., King A., Herbig M., Lauridsen E.M., Johnson G., Marrow T.J. and Buffière J.Y. (2009) Three-dimensional grain mapping by x-ray diffraction contrast tomography and the use of Friedel pairs in diffraction data analysis. *Review of Scientific Instruments*, **80**, 033905.

Maitland T. and Sitzman S. (2007) *Electron backscatter diffraction (EBSD) technique and materials characterization examples*. P. in.: Springer Berlin.

McDonald S.A., Reischig P., Holzner C., Lauridsen E.M., Withers P.J., Merkle A.P. and Feser M. (2015) Non-destructive mapping of grain orientations in 3D by laboratory X-ray microscopy. *Scientific Reports*, **5**.

McDonald S.A., Holzner C., Lauridsen E.M., Reischig P., Merkle A.P. and Withers P.J. (2017) Microstructural evolution during sintering of copper particles studied by laboratory diffraction contrast tomography (LabDCT). *Scientific Reports*, **7**, 5251.

Michibayashi K., Mainprice D., Fujii A., Uehara S., Shinkai Y., Kondo Y., Ohara Y., Ishii T., Fryer P., Bloomer S.H., Ishiwatari A., Hawkins J.W. and Ji S. (2016) Natural olivine crystal-fabrics in the western Pacific convergence region: A new method to identify fabric type. *Earth and Planetary Science Letters*, **443**, 70–80.

Miyamoto M., Mikouchi T. and Jones R.H. (2009) Cooling rates of porphyritic olivine chondrules in the Semarkona (LL3. 00) ordinary chondrite: A model for diffusional equilibration of olivine during fractional crystallization. *Meteoritics & Planetary Science*, **44**, 521–530.

Mizukami T., Wallis S.R. and Yamamoto J. (2004) Natural examples of olivine lattice preferred orientation patterns with a flow-normal a-axis maximum. *Nature*, **427**, 432.

Niverty S., Sun J., Williams J., Bachmann F., Gueninchault N., Lauridsen E.M. and Chawla N. (2019) A Forward Modeling Approach to High Reliability Grain Mapping by Laboratory Diffraction Contrast Tomography (LabDCT). *The Journal of The Minerals, Metals & Materials Society*, 1–10.

Oddershede J., Sun J., Gueninchault N., Bachmann F., Bale H., Holzner C. and Lauridsen E. (2019) Non-destructive Characterization of Polycrystalline Materials in 3D by Laboratory Diffraction Contrast Tomography. *Integrating Materials and Manufacturing Innovation*.

Pankhurst M.J., Dobson K.J., Morgan D.J., Loughlin S.C., Thordarson T., Courtios L. and Lee P.D. (2014) Directly monitoring the magmas fuelling volcanic eruptions in near-real-time using X-ray micro-computed tomography. *Journal of Petrology*, **55**, 671–684.

Pankhurst M.J., Walshaw R. and Morgan D.J. (2017) Major Element Chemical Heterogeneity in Geo2 Olivine Microbeam Reference Material: A Spatial Approach to Quantifying Heterogeneity in Primary Reference Materials. *Geostandards and Geoanalytical Research*, **41**, 85–91.

Pankhurst M.J., Morgan D.J., Thordarson T. and Loughlin S.C. (2018a) Magmatic crystal records in time, space, and process, causatively linked with volcanic unrest. *Earth and Planetary Science Letters*, **493**, 231–241.

Pankhurst M.J., Vo N.T., Butcher A.R., Long L., Wang H., Nonni S., Harvey J., Guðfinnsson G., Fowler R., Atwood R., Walshaw R. and Lee P.D. (2018b) Quantitative measurement of olivine composition in three dimensions using helical scan X-ray micro tomography. *American Mineralogist*, **103**, 1800–1811.

Piatak N.M., Parsons M.B. and Seal R.R. (2015) Characteristics and environmental aspects of slag: A review. *Applied Geochemistry*, **57**, 236–266.

Piazolo S., Austrheim H. and Whitehouse M. (2012) Brittle-ductile microfabrics in naturally deformed zircon: Deformation mechanisms and consequences for U-Pb dating. *American Mineralogist*, **97**, 1544–1563.

Poulsen H.F. (2012) An introduction to three-dimensional X-ray diffraction microscopy. *Journal of Applied Crystallography*, **45**, 1084–1097.

Poulsen H.F., Nielsen S.F., Lauridsen E.M., Schmidt S., Suter R.M., Lienert U., Margulies L., Lorentzen T. and Juul Jensen D. (2001) Three-dimensional maps of grain boundaries and the stress state of individual grains in polycrystals and powders. *Journal of Applied Crystallography*, **34**, 751–756.

Prior D.J., Mariani E. and Wheeler J. (2009) EBSD in the Earth Sciences: Applications, Common Practice, and Challenges. Pp. 345–360 in: *Electron Backscatter Diffraction in Materials Science* (A.J. Schwartz, M. Kumar, B.L. Adams and D.P. Field, editors). Springer US, Boston, MA.

Reddy S.M., Timms N.E., Pantleon W. and Trimby P. (2007) Quantitative characterization of plastic deformation of zircon and geological implications. *Contributions to Mineralogy and Petrology*, **153**, 625–645.

Rudraswami N.G., Prasad M.S., Jones R.H. and Nagashima K. (2016) In situ oxygen isotope compositions in olivines of different types of cosmic spherules: An assessment of relationships to chondritic particles. *Geochimica Et Cosmochimica Acta*, **194**, 1–14.

Shahani A.J., Bale H., Gueninchault N., Merkle A. and Lauridsen E.M. (2017) Integrated Imaging in Three Dimensions: The Sum is Greater than the Parts. 2.

Shea T., Costa F., Krimer D. and Hammer J.E. (2015a) Accuracy of timescales retrieved from diffusion modeling in olivine: A 3D perspective. *American Mineralogist*, **100**, 2026–2042.

Shea T., Lynn K.J. and Garcia M.O. (2015b) Cracking the olivine zoning code: Distinguishing between crystal growth and diffusion. *Geology*, **43**, 935–938.

Spiess R., Bertolo B., Borghi A. and Centi M.T. (2001) Crustal-mantle lithosphere decoupling as a control on Variscan metamorphism in the Eastern Alps. *Australian Journal of Earth Sciences*, **48**, 479–486.

Spiess R., Groppo C. and Compagnoni R. (2007) When epitaxy controls garnet growth. *Journal of Metamorphic Geology*, **25**, 439–450.

Spiess R., Dibona R., Rybacki E., Wirth R. and Dresen G. (2012) Depressurized Cavities within High-strain Shear Zones: their Role in the Segregation and Flow of SiO2-rich Melt in Feldspar-dominated Rocks. *Journal of Petrology*, **53**, 1767–1776.

Storey C.D. and Prior D.J. (2005) Plastic Deformation and Recrystallization of Garnet: A Mechanism to Facilitate Diffusion Creep. *Journal of Petrology*, **46**, 2593–2613.

Sun J., Zhang Y., Lyckegaard A., Bachmann F., Lauridsen E.M. and Juul Jensen D. (2019) Grain boundary wetting correlated to the grain boundary properties: A laboratory-based multimodal X-ray tomography investigation. *Scripta Materialia*, **163**, 77–81.

Tasaka M., Michibayashi K. and Mainprice D. (2008) B-type olivine fabrics developed in the fore-arc side of the mantle wedge along a subducting slab. *Earth and Planetary Science Letters*, **272**, 747–757.

Timms N.E., Reddy S.M., Fitz Gerald J.D., Green L. and Muhling J.R. (2012) Inclusion-localised crystal-plasticity, dynamic porosity, and fast-diffusion pathway generation in zircon. *Journal of Structural Geology*, **35**, 78–89.

Timms N.E., Erickson T.M., Pearce M.A., Cavosie A.J., Schmieder M., Tohver E., Reddy S.M., Zanetti M.R., Nemchin A.A. and Wittmann A. (2017) A pressure-temperature phase diagram for zircon at extreme conditions. *Earth-Science Reviews*, **165**, 185–202.

Trimby P.W., Prior D.J. and Wheeler J. (1998) Grain boundary hierarchy development in a quartz mylonite. *Journal of Structural Geology*, **20**, 917–935.

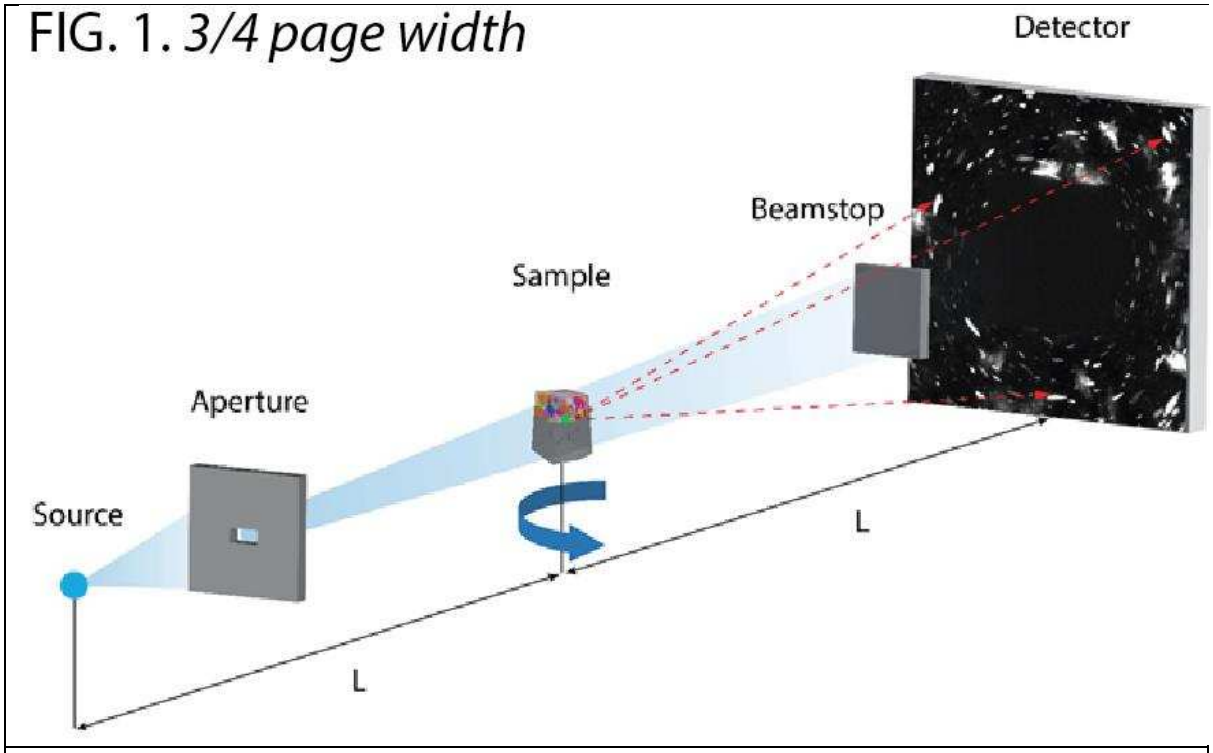

Fig. 1 **Schematic of the experimental setup of LabDCT in the laboratory x-ray microscope** (from Niverty *et al.*, 2019; Oddershede *et al.*, 2019). The location and intensity of diffracted x-rays are recorded as the sample is rotated through 360°. A polychromatic x-ray beam illuminates a region of interest using an aperture between source and sample (distance of L). Transmitted x-rays are not collected due to the placement of a beamstop between sample and detector (distance also L). The transmitted x-rays are substantially stronger and would otherwise flood the detector when using the settings needed to achieve adequate signal:noise for the diffracted x-rays. Diffraction images are focussed by applying Laue geometry and appear as line-shaped spots.

FIG. 2. *3/4 page width*

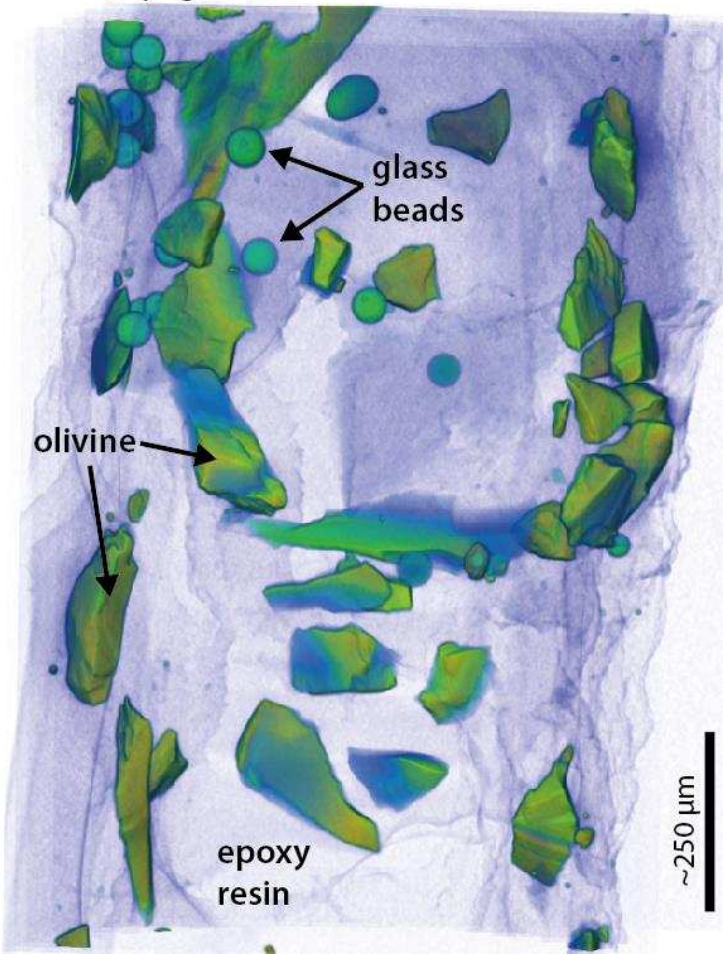

Fig. 2. Tomographic X-ray absorption image of the sample used in the DCT experiment. The view is of the sample as presented to the beam. A qualitative measure of density is illustrated by using a semi-transparent colour-drape over a volume render. Purple is low density, and green-orange is higher density. The edges of the particles are clearly defined against the cured resin, from which their shapes are observed and the particle type identified.

FIG. 3. *full page width*

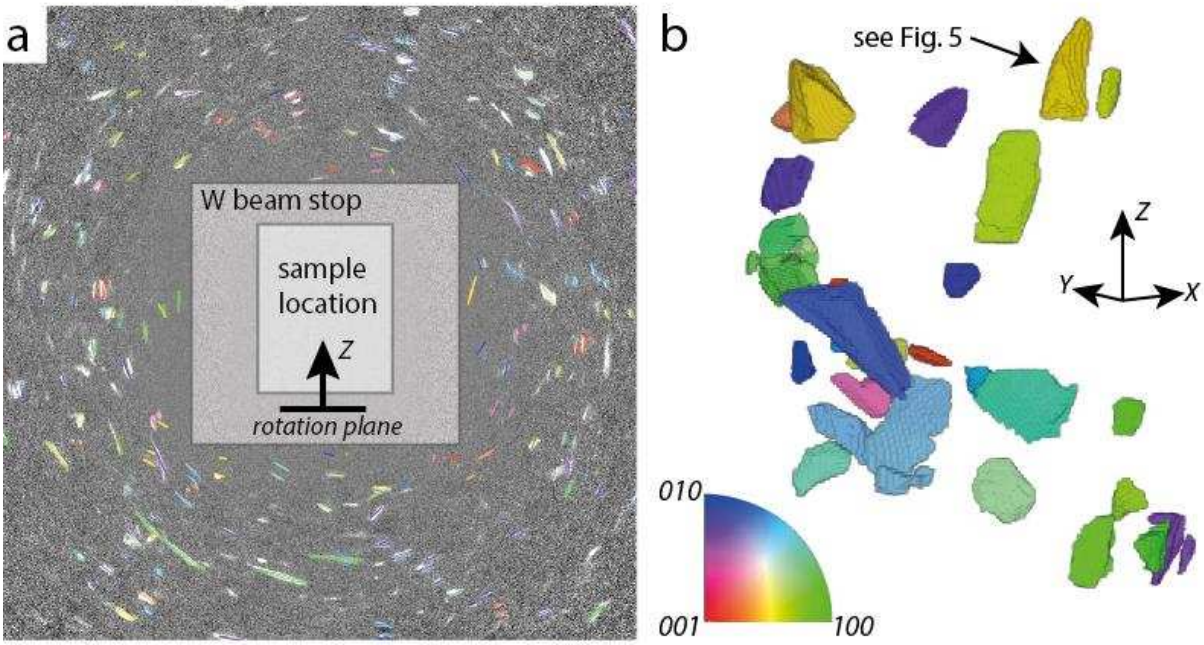

Fig. 3. Example diffraction projection and reconstructed crystallographic orientation tomogram: (*a*) a beamstop (tungsten shield) blocks X-rays from the principle beam (located at the viewer's perspective here) from reaching the square detector, upon which diffraction spots originating from crystals within the sample (in front of the mask) form, and are captured at each sample rotation angle. The intensity, size and shape of the spots are a function of the size and shape and orientation of the particle. The angles between spots, and their shift with sample rotation, contain crystal system and location information; (*b*) the reconstructed volume is labelled according to IPF notation and corresponding inset colourmap. Data are plotted relative to the Z axis, which is the rotation axis. For instance, the 100 axis of dark green crystals are aligned with the Z axis of the sample.

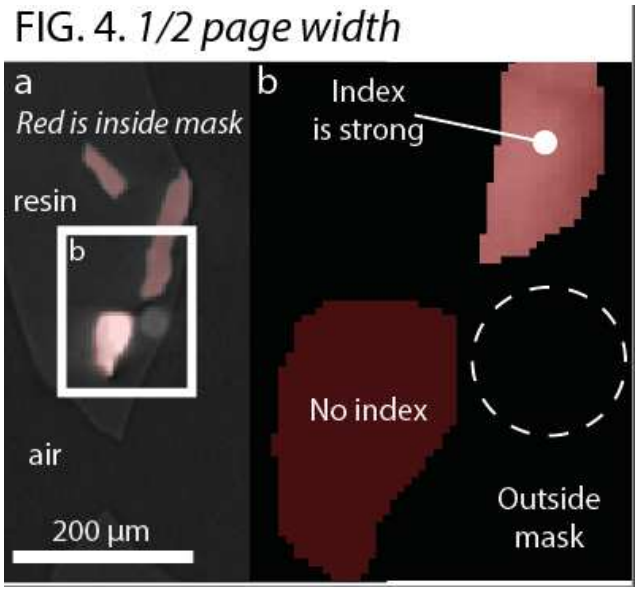

Fig. 4. Crystallographic orientation index quality per material. (*a*) Orthoslice from 3D absorption image overlain with mask defining voxels to attempt indexation. Four particles, resin and air are represented in this view. Three of those particles are resolved from the diffraction data, which indicate they are crystalline. (*b*) Larger view of inset in a: The bright (dense) material in (*a*) is unable to be indexed using an orthorhombic system, whereas the moderately dense particles are indexed with high confidence. Dashed circle approximates the location of the glass microbead.

FIG. 5. *full page width*

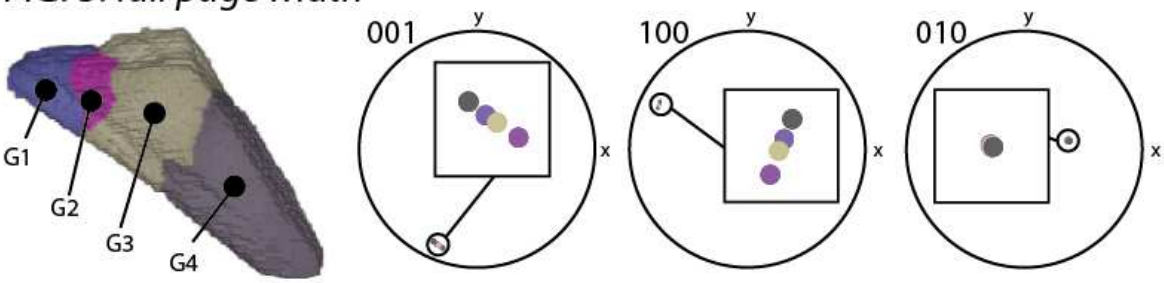

Fig. 5. Detection and quantification of olivine sub-grains in three dimensions. A HKL scheme applied to the diffraction data reveals distinct domains of crystallographic orientation. Each domain is composed of hundreds of voxels that are under a threshold of 0.1 degree of (total) misorientation from each other.

Table 1. Crystallographic measurements from a single fragment of olivine composed of four subgrains shown in Fig. 4: (a) orientation data; (b) misorientation calculations between subgrains.

Orientation (Euler angles in degrees)				**Misorientation**				
Grain	**φ1**	**ψ**	**φ2**		**Angle (degrees)**	**Axis in crystal coordinates**		
G1	336.3	76.78	339.5	**G1/G2**	1.65	<–0.04	0.99	0.07>
G2	337.86	77.28	339.27	**G1/G3**	0.54	<–0.09	–0.15	0.98>
G3	336.83	76.92	339.46	**G2/G3**	1.06	<–0.02	0.99	–0.04>
G4	335.44	76.43	339.65	**G3/G4**	1.44	<–0.01	–0.99	–0.09>

FIG. 6. *full page width*

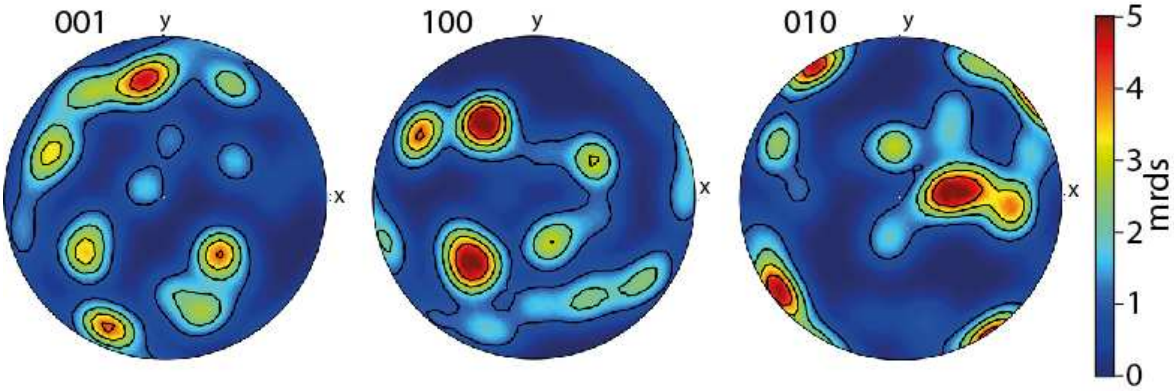

Fig. 6. Pole figures of the olivine data. The spread in all crystallographic orientations demonstrates the random orientation of olivine fragments. Clustering illustrates the contribution of numerous sub-grains with small, yet detectable misorientations.

FIG. 1. *3/4 page width*

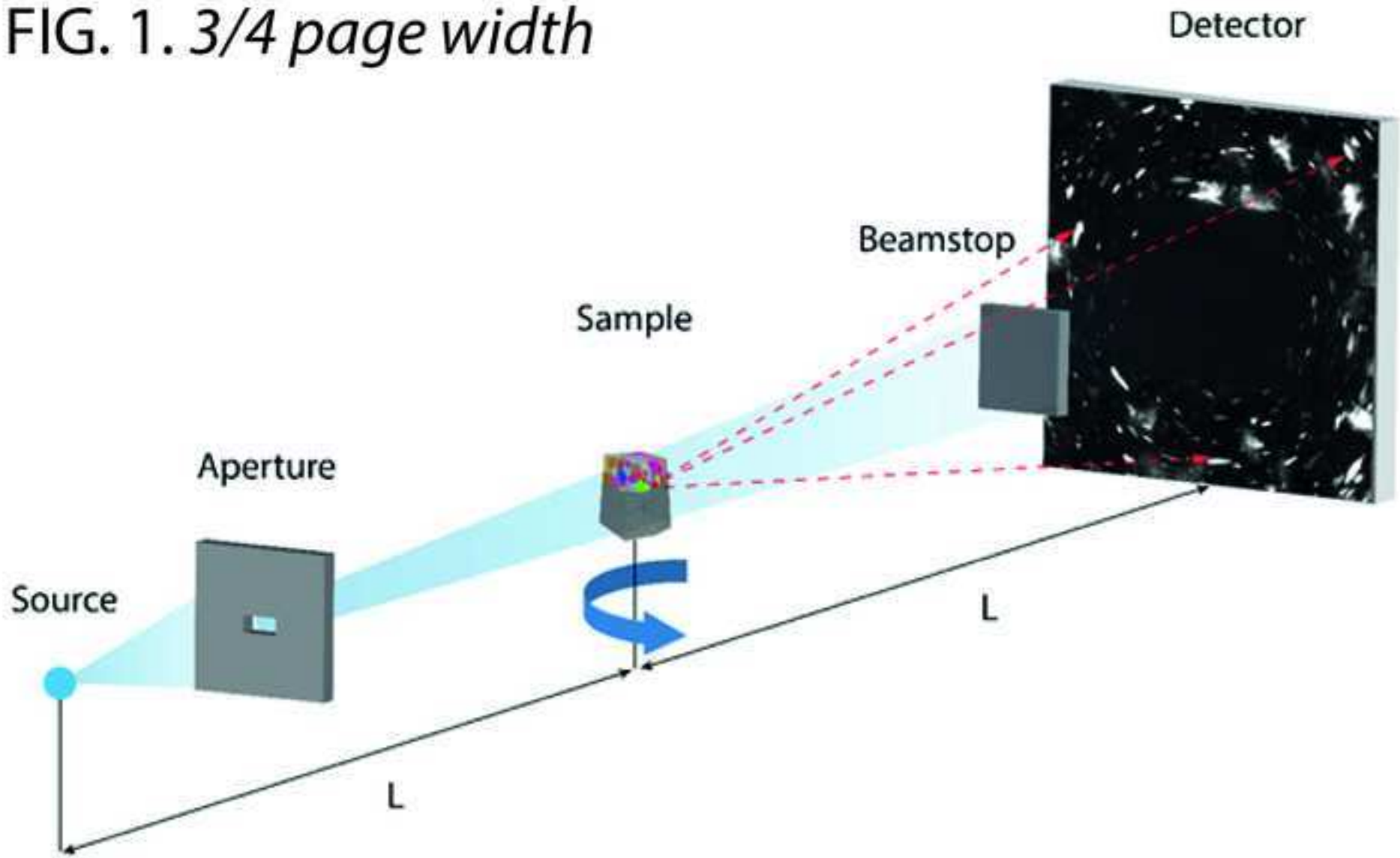

FIG. 2. *3/4 page width*

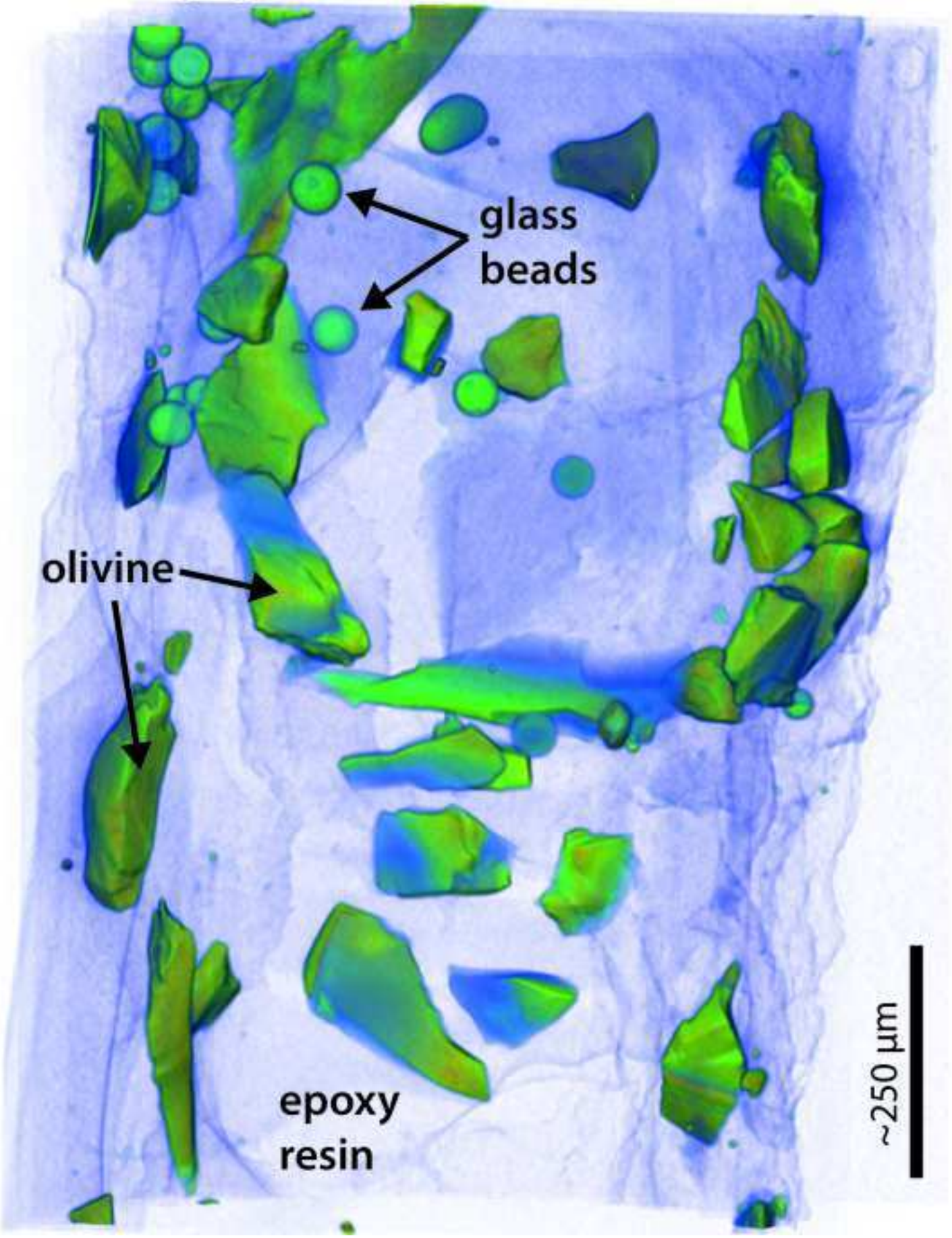

FIG. 3. *full page width*

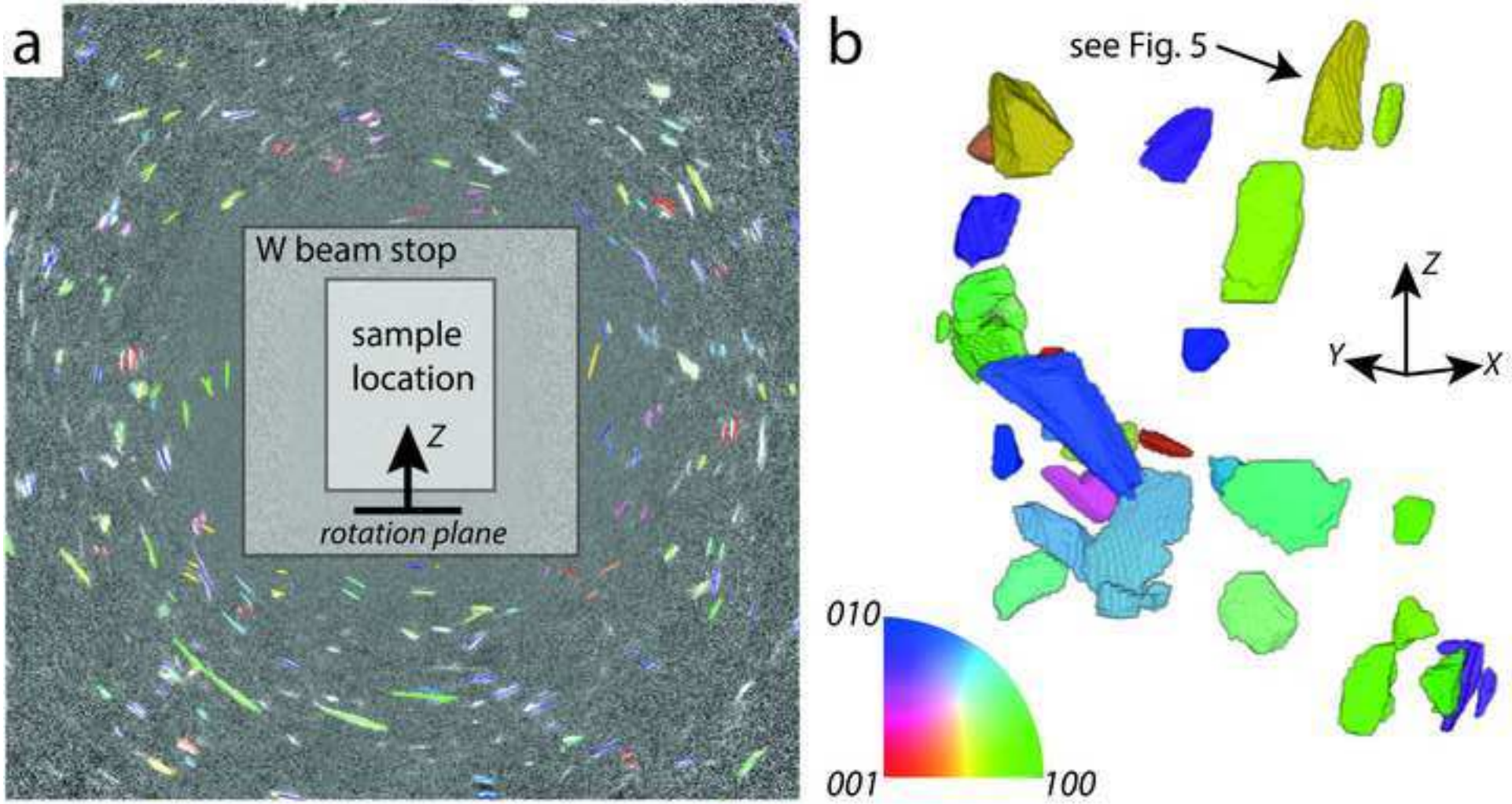

FIG. 4. *1/2 page width*

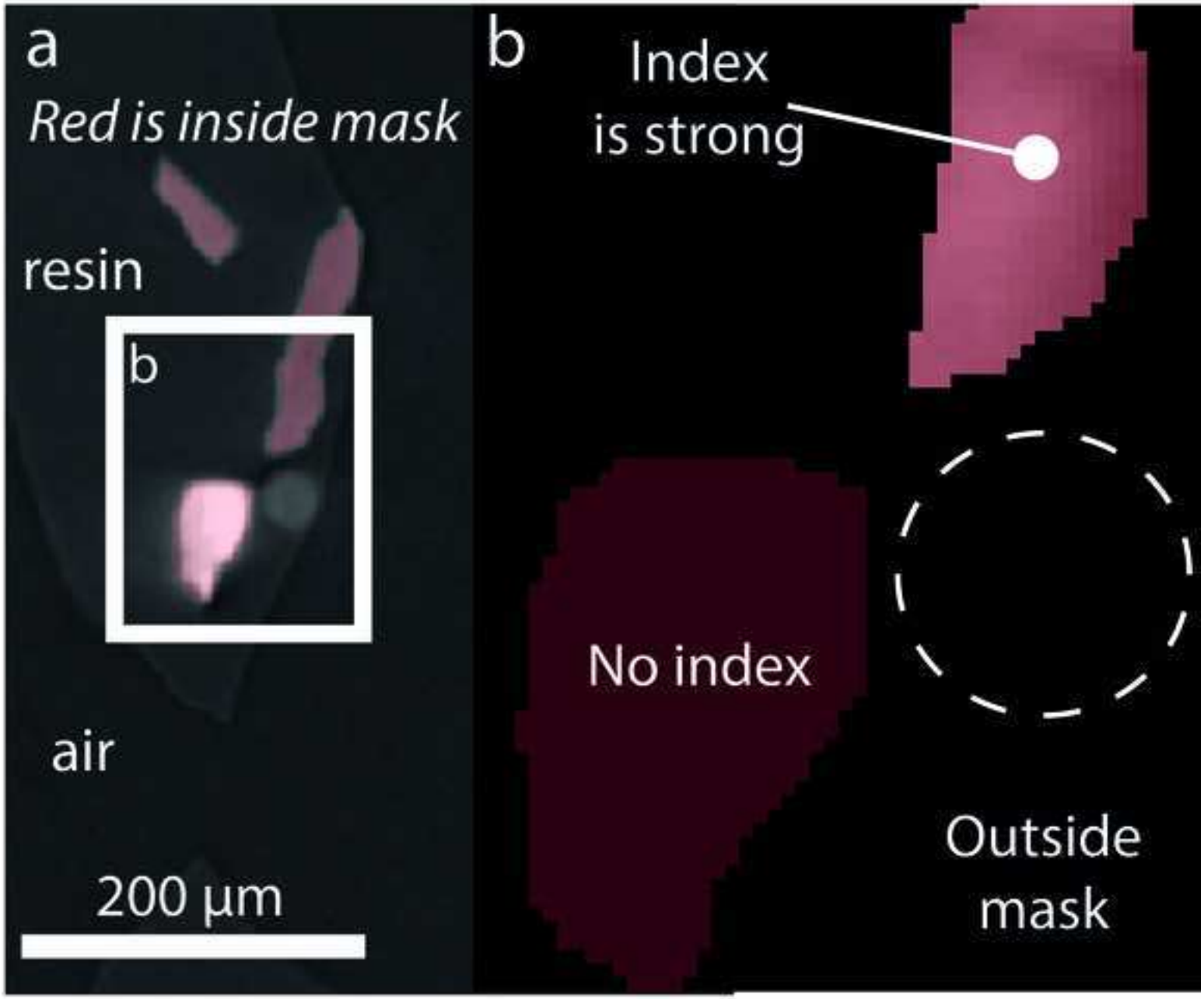

FIG. 5. *full page width*

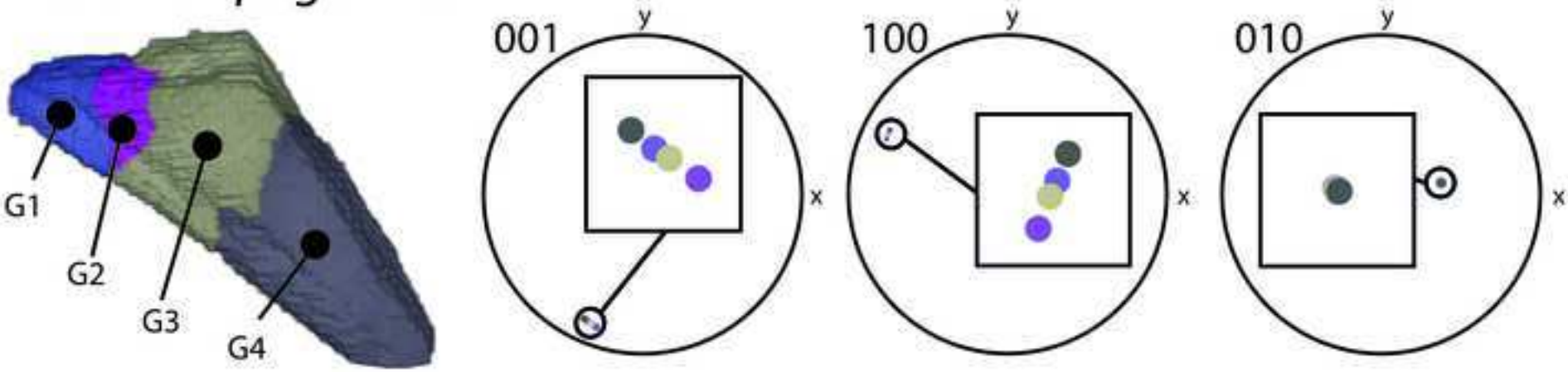

FIG. 6. *full page width*